

Defect removal by solvent vapor annealing in thin films of lamellar diblock copolymers

Xinpeng Xu,^{1,*} Xingkun Man,^{2,3,†} Masao Doi,^{2,3}

Zhong-can Ou-Yang,⁴ and David Andelman⁵

¹*Physics Program, Guangdong Technion – Israel Institute of Technology,
Shantou, Guangdong Province 515063, P. R. China*

²*Center of Soft Matter Physics and Its Applications,
Beihang University, Beijing 100191, P. R. China*

³*School of Physics and Nuclear Energy Engineering,
Beihang University, Beijing 100191, P. R. China*

⁴*CAS Key Laboratory of Theoretical Physics, Institute of Theoretical Physics,
Chinese Academy of Sciences, Beijing 100190, China*

⁵*Raymond and Beverly Sackler School of Physics and Astronomy,
Tel Aviv University, Ramat Aviv 69978, Tel Aviv, Israel*

(Dated: December 15, 2024)

Abstract

Solvent vapor annealing (SVA) is known to be a simple, low-cost and highly efficient technique to produce defect-free diblock copolymer (BCP) thin films. Not only can the solvent dilute the BCP segmental interactions, but also it can vary the characteristic spacing of the BCP microstructures. We carry out systematic theoretical studies on the effect of adding solvent into lamellar BCP thin films and its evaporation rate on the BCP defect removal in close to order-disorder transition. We find that the increase of the lamellar spacing as is induced by added solvent facilitates more efficient removal of defects. The stability of a particular defect in a lamellar BCP thin film is given in terms of the swelling ratio and the solvent evaporation rate. Our results highlight the mechanisms of SVA in obtaining defect-free BCP thin films, as is desired in nanolithography and other industrial applications.

* E-mail address: xu.xinpeng@gtit.edu.cn

† E-mail address: manxk@buaa.edu.cn

I. INTRODUCTION

Thin films of diblock copolymer (BCP) with extended and defect-free lateral order can serve as ideal templates or scaffolds for fabricating nanoscale functional materials, as is desired in nanolithography and ultrafiltration membrane applications [1–3]. However, when a BCP thin film coats a solid substrate, it is usually kinetically trapped in a nonequilibrium and poorly ordered state with significant amount of defects, hindering the mainstream use of BCP thin films in nanotechnology [1–3]. Further treatments are thus needed to facilitate the fabrication of defect-free microdomains. As examples to techniques that have been developed to tailor the self-assembly behavior of BCP thin films we mentioned electric field alignment [4, 5], shear alignment [6, 7], microwave annealing [8], and thermal annealing [1, 2, 9–15]. Besides these approaches, solvent vapor annealing (SVA) [1, 3, 16–30] has been used to enhance the mobility of the polymer chains, and facilitates the annihilation of defects.

In a typical solvent vapor annealing process [1, 3, 18, 20, 21, 28], the BCP thin film is first exposed to vapors of one or more solvents for certain amount of annealing time. After a swollen and mobile polymer film is formed on the substrate, then it is dried by controlled solvent evaporation. During the film swelling in SVA, solvent molecules diffuse into the thin BCP film and screen (or dilute) the unfavorable interactions between polymer segments, leading to a lower effective Flory-Huggins parameter, χ_{eff} , than its value for dry (no solvent) case [20, 21, 31–33]. Note that $\chi_{\text{eff}}(\phi_s)$ is a function of solvent volume fraction, ϕ_s . In addition, as the polymer mobility is greatly enhanced with increasing ϕ_s , the spacing λ of the microdomains also changes as a function ϕ_s [3, 16–22, 28, 34, 35].

Comparing to conventional thermal annealing (TA), SVA offers several unique advantages for defect annihilation [1, 3, 20]: (i) SVA provides means to anneal BCPs that are sensitive to thermal degradation. (ii) SVA is generally more effective (with shorter annealing time) in removing defects for thin films of high-molecular-weight BCPs. (iii) SVA provides additional controlling parameters for tuning film morphology. For example, solvent molecules allow the segregation χN to vary continuously (by varying the swelling ratio or the solvent volume fraction) over a larger range of values than what could be achieved in TA by just changing temperature. In addition, selective solvent can be used to induce asymmetric swelling between BCP blocks, and thus change the morphology of the BCP film.

Despite the widespread use of SVA, a quantitative understanding of its effects in defect

removal has not yet been established [1, 3, 16, 20, 21, 26–30]. Two principal reasons are that no standardized SVA process has been established, and the connection between the nanostructure formed in the swollen film and the final dried film has not been rigorously formulated. Therefore, it is of interest to perform detailed theoretical studies on the effects of the relevant system parameters during the swelling and removal of solvent in SVA [21, 26, 28–30]. Such parameters include swelling ratio, annealing time, solvent evaporation rates, film thickness, temperature, and solvent selectivity. The understanding of their effects on the morphology of BCP thin films is necessary to finely control the SVA process in order to obtain the desired morphology.

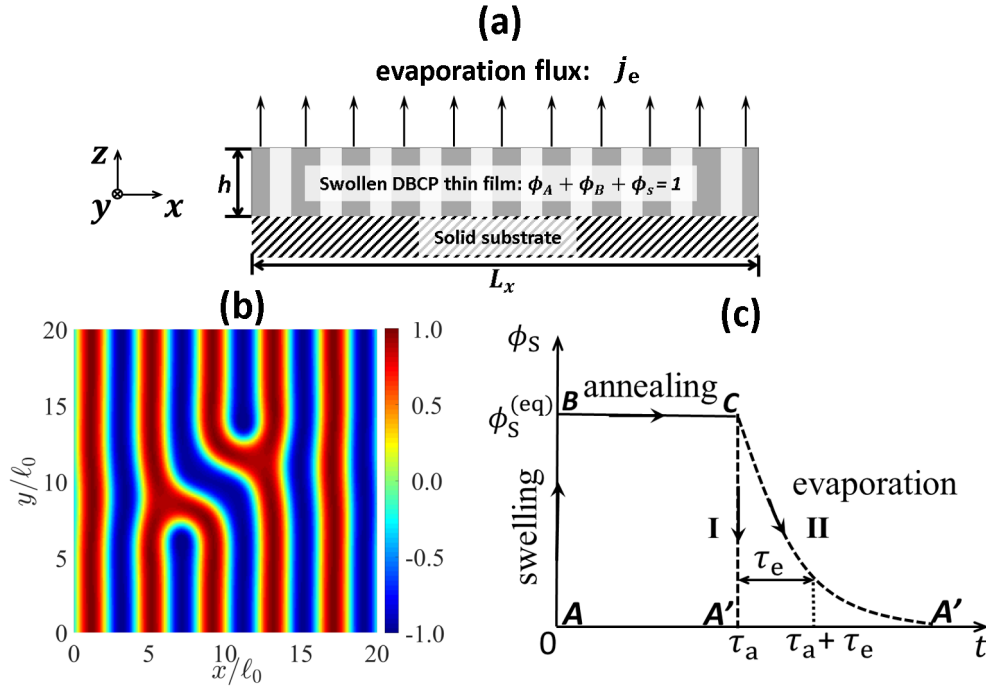


FIG. 1. (a) Schematic illustrations of the BCP film setup, (b) a snapshot of defect structure, and (c) a sketch of the temporal evolution of solvent volume fraction. Three important parameters are shown: the equilibrium solvent fraction, $\phi_S^{(eq)}$, of a swollen film, the annealing time τ_a , and the characteristic evaporation time τ_e . In (c), the lines $A \rightarrow B$, $B \rightarrow C$ and $C \rightarrow A'$ represent the subsequent swelling, annealing and evaporation (deswelling) processes, respectively.

Most previous theoretical and computational studies use either self-consistent field theory or particle-based simulation methods that includes a lot of molecular parameters [26–30]. Here, we propose a continuum two-fluid model for SVA processes in BCP thin films, and carry out detailed numerical analysis on two of the major (dimensionless) system parameters:

(i) Swelling ratio \mathcal{R} , representing the ratio of the swollen film volume V to its original volume V_0 , i.e., $\mathcal{R} \equiv V/V_0$. (ii) Normalized solvent evaporation rate $\alpha_e \equiv \tau_e^{-1}/\tau_0^{-1}$ with τ_e representing the characteristic time for complete evaporation of solvent in the swollen film and τ_0 characterizing the time for copolymer reorganization in the scale of microdomain period λ . To be specific, we investigate the removal of a typical defect occurring in symmetric BCP lamellae in their perpendicular orientation by SVA using non-selective solvent. In experiments of SVA for BCP thin films [16, 20, 21], it has been well established that the swelling ratio and the solvent evaporation rate are the critical annealing parameters and should be specified explicitly. However, a quantitative understanding of their effects on the directed self-assembly using SVA and particularly on the efficiency of SVA in defect removal is still missing. Our main theoretical finding is that the increase of the lamellar spacing induced by added solvent facilitates a more efficient removal of defects in BCP films. Moreover, the dependence of the final morphology of the dried BCP film on \mathcal{R} and α_e is summarized in a stability diagram, which can be verified in future experiments.

II. MODEL AND METHODS

A. Thermodynamics of BCP solutions: Generalized Landau-Brazovskii theory

When a BCP melt is exposed to the vapor of a good solvent, solvent molecules diffuse into the melt to form a swollen BCP solution, in which the chains gain some mobility. Here, specifically, we consider a BCP solution of monodisperse A/B diblocks dissolved in a neutral (non-selective) good solvent for which the polymer-solvent interactions follows $\chi_{AS} = \chi_{BS}$. We restrict ourselves to symmetric A/B BCP where an A-block with N_A monomers is covalently bonded to a B-block with N_B monomers such that $N_A = N_B = N/2$, and N being the polymerization index. Furthermore, for simplicity, we assume incompressibility and zero volume change upon mixing in the BCP solution. In this case, the structure of the BCP solutions can be described by two independent order parameters: the solvent volume fraction ϕ_S with $0 \leq \phi_S \leq 1$ and the relative volume fraction of the two blocks

$$\phi \equiv \phi_A - \phi_B, \quad (1)$$

with $-1 \leq \phi \leq 1$. In addition, since the BCP solution is incompressible, we have

$$\phi_A + \phi_B + \phi_S = 1, \quad \text{or} \quad \phi_P + \phi_S = 1. \quad (2)$$

in which $\phi_P = \phi_A + \phi_B$ is the total volume fraction of A/B copolymer blocks.

It has been known that adding a neutral solvent to the BCP melt has a similar effect on the BCP melt as increasing the temperature [20, 22]. Namely, shifting the phase diagram of BCP melts towards higher temperature in the temperature-composition phase diagram [36]. Based on these understanding, we propose that the structure of a symmetric BCP solution, close to the order-disorder transition (ODT) between the disordered and lamellar phases, can be described by generalizing the Landau-Brazovskii free-energy \mathcal{F} [37–42] (in units of $k_B T$) as

$$\mathcal{F}[\phi, \phi_S] = \int d^3\mathbf{r} \left[f_S(\phi_S) + \frac{\tau}{2}\phi^2 + \frac{u}{4!}\phi^4 + \frac{\kappa}{2}(\nabla^2\phi + q^2\phi)^2 \right], \quad (3)$$

in which we take $f_S(\phi_S) = \phi_S \ln \phi_S - \phi_S$ and the parameters are given by [37–42]

$$\tau \simeq 2\rho N(\chi_c - \chi_{\text{eff}}), \quad u \simeq \rho, \quad \kappa \simeq \frac{6\rho}{q^4}, \quad q \simeq \frac{2}{R_g}, \quad (4a)$$

with $\rho = 1/(Na^3)$ being the copolymer closed packing chain density of an incompressible BCP melt, a the monomer size, $\chi_c N \simeq 10.5$ for the ODT, $R_g^2 = Na^2/6$ the gyration radius for Gaussian chains, and a the monomer size. q is the characteristic wavevector of ordered BCP microdomain, which gives the characteristic domain spacing $\lambda = 2\pi/q$. Note that for a swollen BCP solution with nonselective solvent, the effective interaction parameter χ_{eff} in τ and the domain spacing λ are both functions of the solvent volume fraction, ϕ_S . Firstly, for χ_{eff} , we follow the experimental measurements and take the following power-law form [20, 21, 31–33],

$$\chi_{\text{eff}} = \chi(\phi_P)^\delta = \chi(1 - \phi_S)^\delta, \quad (5)$$

in which the exponent $\delta > 0$ varies from 1.0 to 1.6 for a large range of ϕ_S [31–33], representing the dilution effect of added solvent on the polymer chains by reducing the unfavorable A/B segmental interactions. Particularly, the case with $\delta = 1.0$ can be obtained from the mean field *dilution approximation* [31, 32], by assuming a uniform distribution of solvent throughout the BCP structure. The scaling of λ with the volume fraction of solvent is often approximated by another power law [3, 16–22, 28, 34, 35]

$$\lambda = \lambda_0(\phi_P)^\beta = \lambda_0(1 - \phi_S)^\beta, \quad (6)$$

which represents the effects of added solvent on the microdomain spacing λ of the BCP solution. Here β is a characteristic (either positive or negative) parameter of BCP solutions [3, 16–22, 28, 34, 35] that depends on the degree of solvent selectivity, solvent volume fraction, and morphology of the ordered state. It is known from previous studies in both bulk BCP solutions [34, 35] and BCP films [3, 20–22] that the solvent-induced changes in lamellar spacing can be classified into two regimes according to the solvent volume fraction ϕ_s , which are separated by a crossover solvent volume fraction ϕ_s^* , another characteristic parameter of the BCP solution (*e.g.*, $\phi_s^* \approx 0.3$ for both polystyrene-polyisoprene (PS-PI) and polystyrene-poly(2-vinyl pyridine) (PS-P2VP) copolymers in solutions with non-selective solvent [20, 21, 34]):

- *Kinetically controlled regime* with $\beta < 0$ for dense polymer solutions with $\phi_s < \phi_s^*$, which represents that the lamellar spacing λ increases with increasing solvent fraction. In this regime, λ is kinetically controlled [22, 34, 35] in the sense that the copolymers does not gain much motility, the BCP structure reorganization cannot take place in a typical annealing time, and further addition of solvent therefore results in expansion in all directions. For example, it can be obtained from solvent volume conservation that $\beta = -1/3$ for an isotropic swelling and $\beta = -1$ for a uniaxial swelling of a (dense) BCP solution.
- *Thermodynamically controlled regime* with $\beta > 0$ for dilute polymer solutions with $\phi_s > \phi_s^*$, which represents that the lamellar spacing decreases with increasing solvent fraction. This results from the decrease in segregation magnitude as seen in eq. (5) [3, 20–22]. For large ϕ_s , λ is thermodynamically controlled [20–22, 34, 35] in the sense that the copolymers are sufficiently mobile and expand efficiently (by significant expansion of the average distance between the chemical junction points) along the lamellae interface for a given annealing time. Any addition of solvent can then result in a decrease of the domain spacing λ *perpendicular* to the interface. For example, it was found experimentally that $\beta \approx 1/3$ in dilute BCP bulk solutions of PS-PI with nonselective solvents [34, 35] and $\beta \approx 2/3$ in dilute BCP solution films of PS-P2VP with nonselective solvents [20, 21].

The equilibrium structure of a swollen BCP solution is then given by the minimization of the Landau-Brazovskii free-energy \mathcal{F} with respect to ϕ and ϕ_s subject to the constraint

of conserved solvent fraction ϕ_S and phase parameter ϕ :

$$\mu_S \equiv \frac{\delta \mathcal{F}}{\delta \phi_S} = \ln \phi_S = \text{const.} \quad (7a)$$

$$\mu_\phi \equiv \frac{\delta \mathcal{F}}{\delta \phi} = \tau \phi + u \phi^3 + \kappa(q^4 \phi + 2q^2 \nabla^2 \phi + \nabla^4 \phi) = \text{const.} \quad (7b)$$

with boundary conditions given at the neutral solid surface by

$$\hat{\mathbf{n}} \cdot \nabla \phi = 0, \quad (8a)$$

$$\hat{\mathbf{n}} \cdot \nabla (\nabla^2 \phi + q^2 \phi) = 0, \quad (8b)$$

and at the film-air interface

$$\nabla^2 \phi + q^2 \phi = 0, \quad (8c)$$

$$\hat{\mathbf{n}} \cdot \nabla (\nabla^2 \phi + q^2 \phi) = 0. \quad (8d)$$

Here $\hat{\mathbf{n}} = (-\nabla_{\parallel} h, 1)/\sqrt{1 + (\nabla_{\parallel} h)^2}$ is the normal unit vector of the film-air interface ($\mathbf{u} \cdot \nabla_{\parallel} h$ with ∇_{\parallel} being the 2D velocity vector gradient operator in the xy -plane. Note that in eq. (7a) we have neglected the contribution from the concentration-dependence of τ and q as shown in eq. (4a). This is equivalent to neglecting the influence of copolymers on the chemical equilibrium of solvent. The resulting equilibrium distribution is consistent with the assumption of uniform distribution of solvent through the BCP films. In addition, we would like to point out that the Landau-Brazovskii free-energy (3) can be further extended to include more physical effects by introducing more terms, *e.g.*, solvent selectivity by coupling term $c\phi_S\phi$ (with $c > 0$ representing representing B-preferred solvent), solvent accumulation at A/B interface by gradient term $(\nabla\phi_S)^2$, and Marangoni effects by a concentration-dependent rigidity $\kappa(\phi_S)$.

In addition, we would like to point out that, close to the ODT, the BCP system is described by two lengths: (i) the periodic spacing of BCP microdomain $\lambda = 2\pi/q$, and (ii) the correlation length $\xi \sim (\tau/\kappa)^{-1/4} \sim \lambda(\chi_{\text{eff}}N - \chi_c N)^{-1/4}$, characterizing the decay of modulations and diverging at the ODT, $\chi = \chi_c$. In particular, for BCP films below the

ODT ($\tau < 0$ or $\chi_{\text{eff}}N > \chi_c N$), a defect-free perpendicular lamellar state can be described in the single-mode approximation (in the limit of weak segregation, $\chi_{\text{eff}}N \geq \chi_c N$) by

$$\phi = \phi_q \cos(qx), \quad (9)$$

with $\phi_q \sim \sqrt{8\tau/u} = 4(\chi_{\text{eff}}N - \chi_c N)^{1/2}$ being the amplitude obtained by minimizing free energy with respect to ϕ_q , and $\lambda = 2\pi/q$ is the periodic spacing of the lamellae.

Finally, it is worthwhile to mention that Ohta and Ito [43] have constructed another Landau-type free energy to describe the microphase separation of general BCP-homopolymer mixtures. This, therefore, provides an alternative free energy model of BCP solutions by simplifying homopolymers to small solvent molecules.

B. Dynamics of BCP solutions: Two-fluid model

With the generalized Landau-Brazovskii free-energy, we formulate a two-fluid model for the BCP solutions with non-selective solvent to explore the dynamic coupling between BCP copolymers and small solvent molecules during SVA. This is in analogy to a two-fluid model used to model polymer solutions, polymer blends, and diblock copolymer melts [44–49].

Let's consider a BCP solution in which bulk flow and diffusion are taking place simultaneously, *i.e.*, the velocity of the A/B blocks differ from each other and from the solvent velocity. First, from the conservation of solvent and A/B blocks we have

$$\partial_t \phi_j = -\nabla \cdot (\phi_j \mathbf{v}_j), \quad (10)$$

where $j = \text{s, A, B}$ represents the three components: solvent, A-block and B-block, respectively; \mathbf{v}_j and ϕ_j are the average velocities and volume fractions of each component, respectively. For simplicity, we assume incompressibility as given in eq. (2) and zero volume change upon mixing in the BCP solution, from which we obtain

$$\nabla \cdot \mathbf{v} = 0. \quad (11)$$

with the volume averaged velocity \mathbf{v} defined by $\mathbf{v} \equiv \phi_{\text{s}}\mathbf{v}_{\text{s}} + \phi_{\text{A}}\mathbf{v}_{\text{A}} + \phi_{\text{B}}\mathbf{v}_{\text{B}}$.

From eqs. (10) and (11) we obtain

$$\begin{aligned} \partial_t \phi_{\text{s}} + \mathbf{v} \cdot \nabla \phi_{\text{s}} &= -\nabla \cdot \mathbf{j}_{\text{s}}, \\ \partial_t \phi + \mathbf{v} \cdot \nabla \phi &= -\nabla \cdot \mathbf{j}_{\phi}, \end{aligned} \quad (12)$$

where

$$\begin{aligned}
\phi_A &= (1 - \phi_S + \phi)/2, \\
\phi_B &= (1 - \phi_S - \phi)/2, \\
\mathbf{j}_S &\equiv \phi_S (\mathbf{v}_S - \mathbf{v}) = -\phi_A (\mathbf{v}_A - \mathbf{v}) - \phi_B (\mathbf{v}_B - \mathbf{v}), \\
\mathbf{j}_\phi &\equiv \phi_A (\mathbf{v}_A - \mathbf{v}) - \phi_B (\mathbf{v}_B - \mathbf{v}).
\end{aligned} \tag{13}$$

Note that ϕ_S and ϕ are both conserved order parameters of the BCP solution.

To determine \mathbf{v} , \mathbf{j}_S , and \mathbf{j}_ϕ , we employ Onsager's variational principle [44–48, 50], in which the Rayleighian functional is given by $\mathcal{R} = \dot{\mathcal{F}} + \Phi$ with the change rate of free energy given by

$$\dot{\mathcal{F}} = \int d^3\mathbf{r} (\mu_\phi \partial_t \phi + \mu_S \partial_t \phi_S). \tag{14}$$

The dissipation function is generally given by

$$\Phi = \int d^3\mathbf{r} \left[\frac{1}{2} \sum_{i,j} \tilde{\zeta}_{ij} \mathbf{v}_i \cdot \mathbf{v}_j + \frac{\zeta_S}{2} (\mathbf{v}_B - \mathbf{v}_S)^2 + \frac{\eta}{4} (\nabla \mathbf{v} + \nabla \mathbf{v}^T)^2 \right], \tag{15}$$

where $i, j = A, B, S$ and the friction matrix $\tilde{\zeta}_{ij}$ must be symmetric. Furthermore, since Φ has to be invariant under Galilean transformation, we get

$$\sum_i \tilde{\zeta}_{ij} = 0, \quad \sum_j \tilde{\zeta}_{ij} = 0, \tag{16}$$

and hence there are only *three* independent components in $\tilde{\zeta}_{ij}$. Therefore, we can rewrite the Galilean-invariant dissipation function into the following form

$$\Phi = \int d^3\mathbf{r} \left[\frac{\zeta}{2} (\mathbf{v}_A - \mathbf{v}_B)^2 + \frac{\zeta_S}{2} (\mathbf{v}_A - \mathbf{v}_S)^2 + \frac{\zeta_S}{2} (\mathbf{v}_B - \mathbf{v}_S)^2 + \frac{\eta}{4} (\nabla \mathbf{v} + \nabla \mathbf{v}^T)^2 \right], \tag{17a}$$

or equivalently

$$\Phi = \int d^3\mathbf{r} \left[\frac{1}{2} L_{\phi\phi} \mathbf{j}_\phi^2 + \frac{1}{2} L_{\phi S} \mathbf{j}_\phi \cdot \mathbf{j}_S + \frac{1}{2} L_{S\phi} \mathbf{j}_\phi \cdot \mathbf{j}_S + \frac{1}{2} L_{SS} \mathbf{j}_S^2 + \frac{\eta}{4} (\nabla \mathbf{v} + \nabla \mathbf{v}^T)^2 \right], \tag{17b}$$

where the resistance matrix L_{ij} (with $i, j = S, \phi$) is given by

$$\begin{aligned}
L_{\phi\phi} &= 4\zeta(1 - \phi_S)^2 + \zeta_S [(1 - \phi_S + \phi)^2 + (1 - \phi_S - \phi)^2], \\
L_{\phi S} &= L_{S\phi} = 4\zeta\phi(1 - \phi_S) + \frac{\zeta_S}{\phi_S} [(1 - \phi)(1 - \phi_S + \phi)^2 - (1 + \phi)(1 - \phi_S - \phi)^2], \\
L_{SS} &= 4\zeta\phi^2 + \frac{\zeta_S}{\phi_S^2} [(1 - \phi)^2(1 - \phi_S + \phi)^2 + (1 + \phi)^2(1 - \phi_S - \phi)^2].
\end{aligned} \tag{18}$$

Here we have assumed equilibrium conditions as given in eq. (7) at the boundaries of the BCP film. The first three terms in the energy dissipation eq. (17) are caused by the relative motion between the different polymer blocks and between polymer blocks and solvent. The fourth term represents the energy dissipation caused by solvent velocity gradients, where η is the solution viscosity, and ζ and ζ_S are the friction constants per unit volume. Note that for neutral solvents, the friction constants for the relative motion between the A/B blocks. In addition, we would like to point out that the viscoelastic properties of the BCP solution can also be incorporated into the two-fluid model as discussed in Ref. [45] for polymer solutions and blends.

Substituting eq. (12) into eqs. (14) and (17b), minimizing Rayleighian with respect to \mathbf{v} , \mathbf{j}_S , and \mathbf{j}_ϕ and substituting the obtained results back into eqs. (12), we obtain the following set of dynamic equations [44–48, 50]

$$\begin{aligned}\partial_t \phi_S + \mathbf{v} \cdot \nabla \phi_S &= \nabla \cdot [M_{SS} \nabla \mu_S + M_{S\phi} \nabla \mu_\phi], \\ \partial_t \phi + \mathbf{v} \cdot \nabla \phi &= \nabla \cdot [M_{\phi S} \nabla \mu_S + M_{\phi\phi} \nabla \mu_\phi], \\ -\nabla p + \eta \nabla^2 \mathbf{v} - \phi \nabla \mu_\phi - \phi_S \nabla \mu_S &= 0,\end{aligned}\tag{19}$$

with the incompressibility condition (11). Here we have substituted the following constitutive relations resulted from the Rayleighian minimization

$$\begin{aligned}\mathbf{j}_S &= -[M_{SS} \nabla \mu_S + M_{S\phi} \nabla \mu_\phi], \\ \mathbf{j}_\phi &= -[M_{\phi S} \nabla \mu_S + M_{\phi\phi} \nabla \mu_\phi]\end{aligned}\tag{20}$$

into conservation Eqs. (12). The motility coefficient matrix M_{ij} (with $i, j = S, \phi$) is the inverse of the resistance matrix L_{ij} given in eq. (18), which is also symmetric and its elements in the limit of dilute solution (*i.e.*, small solvent fraction) are found to be

$$\mathbf{M} \sim \begin{bmatrix} \zeta_S^{-1} \phi_S^2 & -\zeta_{\text{eff}}^{-1} \phi_S \phi \\ -\zeta_{\text{eff}}^{-1} \phi_S \phi & \zeta_{\text{eff}}^{-1} \end{bmatrix}\tag{21}$$

with the effective friction constant per volume ζ_{eff} depending on the relative values of ζ and ζ_S . It is worthwhile to point out that the copolymer diffusion usually depends on the morphology of the BCP solutions [28, 48, 51]; particularly for lamellar BCP with uniaxial symmetry, anisotropic diffusion is known [48, 51] to be able to enhance or reduce the rate of relaxation of long-wavelength perturbations of lamellae. But here for simplicity, we only consider the case of isotropic diffusion as a typical application of the two-fluid model.

For a thin film of BCP solution, the above set of equations has to be supplemented with proper boundary conditions [50]. At the bottom (neutral) substrate ($z = 0$), we have [50]

$$\begin{aligned}\mathbf{v} &= 0, \\ \hat{\mathbf{n}} \cdot \mathbf{j}_S &= \hat{\mathbf{n}} \cdot \mathbf{j}_\phi = 0, \\ \hat{\mathbf{n}} \cdot \nabla \phi &= 0, \\ \hat{\mathbf{n}} \cdot \nabla (\nabla^2 \phi + q^2 \phi) &= 0,\end{aligned}\tag{22}$$

with \mathbf{j}_S and \mathbf{j}_ϕ given by Eq. (20). At top free surface at $z = h(t)$, we have [50]

$$\begin{aligned}\hat{\mathbf{n}} \cdot \boldsymbol{\sigma} &= 0, \\ \nabla^2 \phi + q^2 \phi &= 0, \\ \hat{\mathbf{n}} \cdot \nabla (\nabla^2 \phi + q^2 \phi) &= 0,\end{aligned}\tag{23}$$

in which $\boldsymbol{\sigma} = -p\mathbf{I} + \eta(\nabla \mathbf{v} + \nabla \mathbf{v}^T)$ is the viscous stress tensor. In addition, at $z = h(t)$, solvent evaporation occurs; from the evaporation flux defined by $j_e \equiv \rho_0(\mathbf{v} - \mathbf{v}_i) \cdot \hat{\mathbf{n}} = \rho_S(\mathbf{v}_S - \mathbf{v}_i) \cdot \hat{\mathbf{n}}$ we can get kinematic boundary conditions as follows

$$\hat{\mathbf{n}} \cdot \mathbf{v} = \partial_t h + j_e / \rho_0,\tag{24}$$

$$\hat{\mathbf{n}} \cdot \mathbf{j}_S = (1 - \phi_S)j_e / \rho_0,\tag{25}$$

$$\hat{\mathbf{n}} \cdot \mathbf{j}_\phi = -\phi j_e / \rho_0.\tag{26}$$

Here the interface velocity satisfies $\mathbf{v}_i \cdot \hat{\mathbf{n}} = \partial_t h$ [50]. We assume the evaporation flux follow the Hertz-Knudsen relation [26, 27]

$$j_e = \rho_0 v_e (\phi_S(h) - \phi_S^{(\text{eq})}),\tag{27}$$

in which $\phi_S^{(\text{eq})}$ is the solvent fraction of a swollen film at equilibrium with the vapor phase, v_e is an adjustable velocity parameter, proportional to mass transfer coefficient, and relates the rate of evaporative loss τ_e^{-1} from the free surface to inter-diffusion of the solvent through the film by $\tau_e^{-1} = v_e / h_0$ with h_0 being the initial thickness of the BCP film. Note that here we have neglected the surface tension, which is usually very small in comparison to the bulk energy of the BCP film. In this case, the free surface of the BCP film stays flat during SVA.

Regardless of the behavior of the BCP properties, the mathematical problem is intrinsically non-linear due to the fact of a moving boundary. Numerical integration may be carried out following a scheme that was successfully employed in some other moving boundary problems [50, 52, 53]. The method consists of the following steps:

- Assume that $\phi(\mathbf{r}, t)$, $\phi_S(\mathbf{r}, t)$, and $\mathbf{v}(\mathbf{r}, t)$ are known at time t . $\phi(\mathbf{r}, t)$, $\phi_S(\mathbf{r}, t)$, and $\mathbf{v}(\mathbf{r}, t)$ satisfy Eqs. (19) and Eq. (27).
- Neglect the dynamic nature of $\phi(\mathbf{r}, t)$, $\phi_S(\mathbf{r}, t)$, and $\mathbf{v}(\mathbf{r}, t)$. The moving boundary $h(x, y, t)$ is extrapolated to the forward time level $t + \Delta t$ by means of an explicit forward difference expression of Eq. (28).
- Let the boundary $h(x, y, t)$ be fixed at the new time level; determine the distributions of $\phi(\mathbf{r}, t)$, $\phi_S(\mathbf{r}, t)$, and $\mathbf{v}(\mathbf{r}, t)$ of the forward time level $t + \Delta t$ satisfying Eqs. (19) and the boundary conditions (22) through Eq. (27).
- Repeat the iteration schemes of the previous second and third steps.

C. Two-dimensional model for thin BCP films

We consider the limit of no macroscopic convection [45, 46] and focus on thin films of concentrated BCP solutions (with relatively small ϕ_S) where the relaxation dynamics throughout the film thickness (z -direction) is much faster than the lateral (xy -plane) dynamics (as schematically shown in Fig. 1a). This limit is justified when the viscous time scale $\tau_v = h_0^2/\nu$ (with ν being the kinematic viscosity of the BCP solution) is much smaller than the evaporative time $\tau_e = h_0/v_e$ for an initially stationary film to evaporate to dry film, i.e., $\tau_v \ll \tau_e$. Furthermore, we focus on the simple case that the evaporation of solvent is *slow* relative to vertical solvent/polymer diffusion, i.e., $\tau_e \gg \tau_S, \tau_P$ with $\tau_S = h_0^2/D_S$ and $\tau_P = h_0^2/D_P$ being the diffusion times through the film thickness of the solvent and the polymer segments, respectively, and D_S and D_P the corresponding collective diffusion constants. In this case, the variations of phase structure, measured by ϕ , and solvent distribution ϕ_S are negligible in the normal (z -) direction, yielding $\phi = \phi(x, y, t)$ and $\phi_S = \phi_S(t)$.

Under such assumptions, the evolution of the film thickness, the integrated solvent frac-

tion, and the phase structure of BCP thin film is written as

$$h = h_0/(1 - \phi_S), \quad (28)$$

$$\partial_t \phi_S = -\tau_e^{-1}(1 - \phi_S)^2(\phi_S - \phi_S^{(\text{eq})}), \quad (29)$$

$$\partial_t \phi = \nabla_{\parallel} \cdot (M_{\phi\phi} \nabla_{\parallel} \mu_{\phi}). \quad (30)$$

where $M_{\phi\phi}$ is the mobility coefficient, and μ_{ϕ} is the chemical potential of the BCP solution.

We consider the limit of no macroscopic convection [45, 46], *i.e.*, $\mathbf{v} = 0$ and focus on dilute solution with small ϕ_S and small surface tension in comparison to the bulk energy. Hence, the film will stay flat with $\hat{\mathbf{n}} = \hat{\mathbf{z}}$ and from Eq. (21), we have $M_{S\phi} = M_{\phi S} \approx 0$, *i.e.*, no cross-coupling between solvent and copolymer dynamics. This limit is justified when the viscous time $\tau_v = h_0^2/\nu$ (with $\nu = \eta/\rho$ being the solution kinematic viscosity) is much smaller than the evaporative time $\tau_e = h_0/v_e$ that is required for an initially stationary film to evaporate to dry film: $\tau_e \gg \tau_v$. Then, the above set of equations reduces to the following 2D Cahn-Hilliard equation [54, 55]:

$$\begin{aligned} \partial_t \phi_S &= -\nabla \cdot \mathbf{j}_S, & \mathbf{j}_S &= -M_{SS} \nabla \mu_S \\ \partial_t \phi &= -\nabla \cdot \mathbf{j}_{\phi}, & \mathbf{j}_{\phi} &= -M_{\phi\phi} \nabla \mu_{\phi}, \end{aligned} \quad (31)$$

supplemented with boundary conditions at the bottom substrate (at $z = 0$)

$$\begin{aligned} \hat{\mathbf{n}} \cdot \mathbf{j}_S &= \hat{\mathbf{n}} \cdot \mathbf{j}_{\phi} = 0, \\ \partial_z \phi &= 0, \\ \partial_z (\nabla^2 \phi + q^2 \phi) &= 0 \end{aligned} \quad (32)$$

and at the top free surface $z = h(t)$,

$$\begin{aligned} \hat{\mathbf{n}} \cdot \mathbf{j}_S &= (1 - \phi_S)j_e/\rho_0, \\ \hat{\mathbf{n}} \cdot \mathbf{j}_{\phi} &= -\phi j_e/\rho_0, \\ \nabla^2 \phi + q^2 \phi &= 0, \\ \partial_z (\nabla^2 \phi + q^2 \phi) &= 0, \end{aligned} \quad (33)$$

with the evaporation flux given by

$$j_e = \rho_0 v_e (\phi_S - \phi_S^{(\text{eq})}). \quad (34)$$

Moreover, the temporal evolution of the film thickness follows

$$\partial_t h + j_e/\rho_0 = 0. \quad (35)$$

In addition, note that for small volume fraction of solvent with $\mu_S \approx 2A_2\phi_S$ and A_2 being the second virial coefficient, the dynamic equation for solvent in Eq. (31) reduces to simple diffusion equation and the collective diffusion constant of solvent is given by $D_S = 2A_2M_{SS} \sim 2A_2\zeta_S^{-1}\phi_S^2$.

We will focus on thin BCP films where the relaxation dynamics through the film thickness (z -direction) is much faster than lateral (xy -plane) dynamics. The variations of ϕ and ϕ_S are then negligible in the normal direction (z -axis). This leads to an order parameter $\phi = \phi(x, y, t)$ and solvent fraction $\phi_S = \phi_S(t)$. Particularly, the volume fraction ϕ_S of solvent (or the volume fraction $\phi_P = 1 - \phi_S$ of copolymers) is simplified to be an (spatially uniform) “external” control parameter (that can have time-variation depending on the rate of evaporation but no variation in space).

In this case, the integrated solvent fraction follows

$$\partial_t(h\phi_S) + j_e/\rho_0 = 0, \quad (36)$$

from which and Eq. (35) we obtain

$$\begin{aligned} h &= h_0/(1 - \phi_S), \\ \partial_t\phi_S &= -\tau_e^{-1}(1 - \phi_S)^2(\phi_S - \phi_S^{(\text{eq})}) \end{aligned} \quad (37)$$

with $\tau_e \equiv h_0/v_e$ representing the characteristic time for complete evaporation of solvent in the swollen film. The volume fraction of solvent ϕ_S is only a time-varying parameter following eq. (37) and the evolution of phase structure is determined by the following two dimensional dynamic equation

$$\partial_t\phi = \nabla_{\parallel} \cdot (M_{\phi\phi}\nabla_{\parallel}\mu_{\phi}). \quad (38)$$

D. Numerical Method and System Setup

Using the classical central finite-difference method [47, 56], we numerically integrate the dynamical equation (6) for the order parameter ϕ , and eq. (5) for the solvent fraction ϕ_S

(in the xy -plane), as is schematically shown in Fig. 1a. The mesh size of our simulation box is chosen to be

$$\ell_0 \equiv (\kappa/u)^{1/4}, \quad (39)$$

from Eq. (4) we obtain $\ell_0 \approx 0.25\lambda_0$. The simulation box size is taken to be $L_x = L_y = 20\ell_0$. Periodic boundary conditions are employed in both directions. Time is measured in units of

$$\tau_0 \equiv \ell_0^2/\rho_c M_{\phi\phi}, \quad (40)$$

which characterizes the time for copolymer reorganization in the scale of microdomain period $\lambda_0 \sim \ell_0$. Note that the number of lamellar periods equals to an integer that is the closest to L_x/λ_0 . It is *five* for $L_x = 20\ell_0$ and dry lamellar spacing $\lambda_0 \approx 4.0\ell_0$, as can be seen in Fig. 1b.

We carry out a numerical study for the effects of solvent swelling and solvent evaporation on the morphology of a dry BCP film with a particular defect as shown in Fig. 1b. The uptake (swelling) rate of solvent usually strongly depends on the morphology of BCP film even for a non-selective solvent [18]. However, in experiments the exposure time to solvent vapor (the annealing time) is usually longer than that required for the film to swell and reach an equilibrium (solvent) volume fraction [18, 20]. In our simulations, we ignore the effects of solvent uptake process and assume “instantaneous” saturation to equilibrium (solvent) volume fraction $\phi_s^{(\text{eq})}$ as schematically shown in Fig. 1c. After an annealing time τ_a , the solvent is removed by a controlled evaporation rate, τ_e^{-1} , according to eq. (5).

III. RESULTS AND DISCUSSION

We present results about the effects of two key parameters on the defect removal during SVA: solvent-swelling ratio \mathcal{R} , that is a monotonic function of equilibrium volume fraction $\phi_s^{(\text{eq})}$, and the normalized solvent-evaporation rate, $\alpha_e = \tau_e^{-1}/\tau_0^{-1}$.

A. Effects of solvent-swelling ratio

The swelling of the film is one-dimensional along the normal z -direction of the film, due to the lateral confinement of fixed area set by periodic boundary conditions, as shown in

Fig. 1a. The swelling ratio $\mathcal{R} \equiv V/V_0$ is then given by

$$\mathcal{R} = h/h_0 = (1 - \phi_S^{(\text{eq})})^{-1} \quad (41)$$

from the conservation of copolymers and eq. (28) with h_0 and h being the film thicknesses of the original dry film and the swollen film, respectively.

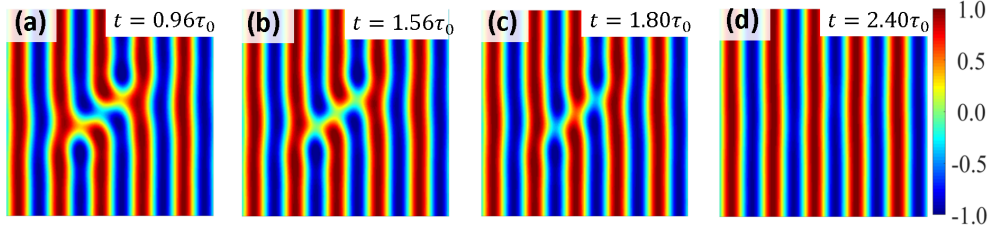


FIG. 2. Defect removal upon instantaneous solvent swelling due to the dilution effects only on χ_{eff} as given in eq. (5), $\chi(1 - \phi_S)$. Here, we take $\chi N = 30$, $\beta = 0.0$ (i.e., no spacing changes induced by solvent), the equilibrium solvent volume fraction $\phi_S^{(\text{eq})} = 0.6$, corresponding to swelling ratio $\mathcal{R} = 2.5$.

As pointed out in the previous section, there are two major effects of a non-selective solvent in a swollen BCP film: diluting effect on $\chi_{\text{eff}}(\phi_S)$, eq. (5), and changing the lamellar spacing $\lambda(\phi_S)$, eq. (6). We first carry out simulations to study a simple case when the solvent-induced changes in lamellar spacing are negligible during solvent annealing. This corresponds to the limit of BCP solutions with $\beta \approx 0$ in Eq. (6), which may result from the weak dependence of either χ_{eff} on ϕ_S or λ on the incompatibility $\chi_{\text{eff}}N$ [20, 21]. The results show that the defect stability strongly depends on the solvent fraction $\phi_S^{(\text{eq})}$ (or swelling ratio \mathcal{R} given in Eq. (41)) in the swollen film.

For a relatively low swelling ratio \mathcal{R} (small $\phi_S^{(\text{eq})}$), the system is kinetically trapped (metastable). In the other limit of very large swelling ratio when $\chi_{\text{eff}} < \chi_c$ (equivalently, $\mathcal{R} > 2.86$ or $\phi_S^{(\text{eq})} > 0.65$), the BCP undergoes an order-disorder transition (ODT), and the BCP solutions evolve to a disordered state without microphase separated structure. As shown in Fig. 2, only in a narrow window of swelling ratio, $2.5 < \mathcal{R} < 2.86$ (or equivalently $0.6 < \phi_S^{(\text{eq})} < 0.65$), the copolymer segments gain large enough mobility but still maintain an ordered structure such that the defect-free lamellar structure is obtained.

It is interesting to note that the mechanism of defect removal by adding solvent to reduce χ is very similar to a thermal annealing (TA) by increasing temperature also reducing

$\chi \sim 1/T$ [2, 9, 10, 12]. Firstly, the presence of a threshold value of incompatibility $\chi_{\text{eff}}N$ (given by a threshold of solvent volume fraction or swelling ratio) in SVA has also been seen in TA ($\chi(T)N$ in TA) [2, 9–13]. For small $\chi_{\text{eff}}N$ (large swelling ratio), defects are not even metastable and removes spontaneously without any barriers to overcome. For large $\chi_{\text{eff}}N$ (small swelling ratio), defects are metastable and some free-energy barriers needs to be overcome. However using our method, we can not quantify the dependence of the energy barrier of the defect on $\chi_{\text{eff}}N$ or ϕ_S . We can only check when the energy barrier of the defect removal vanishes as \mathcal{R} is increased (as discussed above) and examine the dynamic processes of the defect removal.

We found that the dynamic processes of the defect removal in SVA is symmetric in the sense that the two horizontal arms break simultaneously, as seen in Fig. 2a. This is in contrast to the kinetic pathway of defect removal that is predicted in TA, in which the defect removal pathway is asymmetric [9] in the sense that the two horizontal arms in the defect shown in Fig. 1b break sequentially, one by one by crossing two consecutive free energy barriers [11–13].

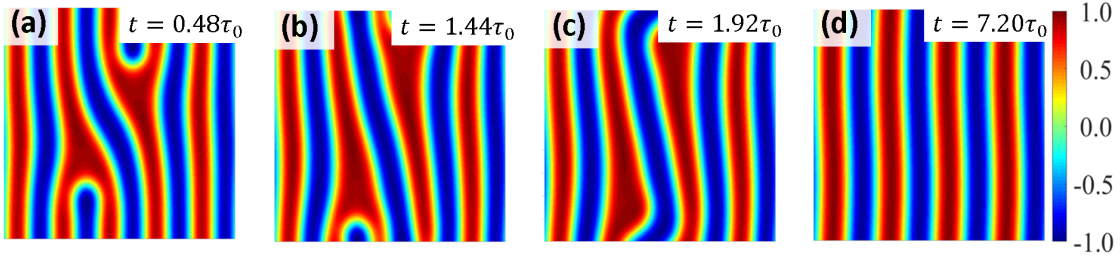


FIG. 3. Destabilization of defects upon instantaneous solvent swelling due to an *increase* in the lamellar spacing. Here, we take $\chi N = 30$, $\phi_S^{(\text{eq})} = 0.4$ ($< \phi_S^*$, corresponding to $\mathcal{R} \approx 1.67$) and $\beta = -1.0$ as defined in Eq. (6). In this case, the energy-preferred number of lamellar periods changes from five (at dry state) to three (at swollen state).

More generally, the change in lamellar spacing λ during solvent annealing of BCP films is visible and cannot be neglected [3, 20, 22]. At small $\phi_S^{(\text{eq})}$ below some critical value ϕ_S^* [34, 35], the spacing λ increases with increasing solvent volume fraction. In Fig. 3 we take $\phi_S^{(\text{eq})} = 0.4$ which is smaller than ϕ_S^* , and $\beta < 0$, the equilibrium lamellar spacing increases from $\lambda_0 \approx 4\ell_0$ for the dry state to $\lambda \approx 6\ell_0$ for the swollen state. Correspondingly, the energy-preferred number of lamellar periods changes from five to three. Fig. 3 shows

that such an increase in lamellar spacing tends to drive long-wavelength structural evolution. Note that after defect removal the system evolves to a metastable defect-free state with four lamellar periods instead of energy-preferred three periods. This again indicates the addition of solvent alters the kinetic pathway of the microstructure evolution of the BCP film.

In addition, comparing these results with spacing changes to those without spacing changes (for example, results shown in Fig. 2), we find that, firstly in both cases, the defect-free state can be obtained only in a narrow window of solvent volume fraction: large enough to make defect state unstable and smaller than ODT to be still in ordered lamellar states. This observation agrees with experiments [16]. Secondly, and more interestingly, the defect structure of BCP solutions with $\phi_S^{(\text{eq})} = 0.4$ is still metastable in the latter case without spacing changes, but becomes unstable in the former case with spacing increases (as shown in Fig. 3). We, therefore, conclude that the solvent-induced increase in lamellar spacing facilitates a more efficient removal of defects.

B. Effects of solvent-evaporation rate

It is well-known that the final morphology of the dried BCP film depends, not only on the swelling ratio \mathcal{R} and the morphology in the swollen state, but also on the evaporation rate of solvent, α_e [3, 18, 20, 22]. To examine this dependence, we carry out simulations for swollen films with different swelling ratio \mathcal{R} (i.e., with different $\phi_S^{(\text{eq})}$) and for solvent evaporation at different rates α_e . As schematically shown in Fig. 1c, the solvent is removed by evaporation following eq. (5) after time τ_a of solvent annealing.

For small swelling ratio $\mathcal{R} < 1.2$ (i.e., $\phi_S^{(\text{eq})} < 0.15$), the amount of solvent in the swollen film is not sufficient to enhance polymer chain mobility such that the original defect is still metastable and kinetically trapped. In the dried film after solvent evaporation, the original defect persists and is found to be independent of the evaporation rate.

In contrast, at large swelling ratio $\mathcal{R} > 2.86$ (i.e., $\phi_S^{(\text{eq})} > 0.65$) where $\chi_{\text{eff}}N < \chi_c N$, the system passes through the ODT and the swollen BCP film is disordered. After the solvent evaporates, the film re-enters the ordered phase but the final dry film is usually trapped in a poorly ordered state with significant amount of defects and the detailed phase structures strongly depend on the evaporation rates. To obtain a defect-free state, one has to direct the film morphology by well controlling the solvent evaporation rate [25–27], or applying

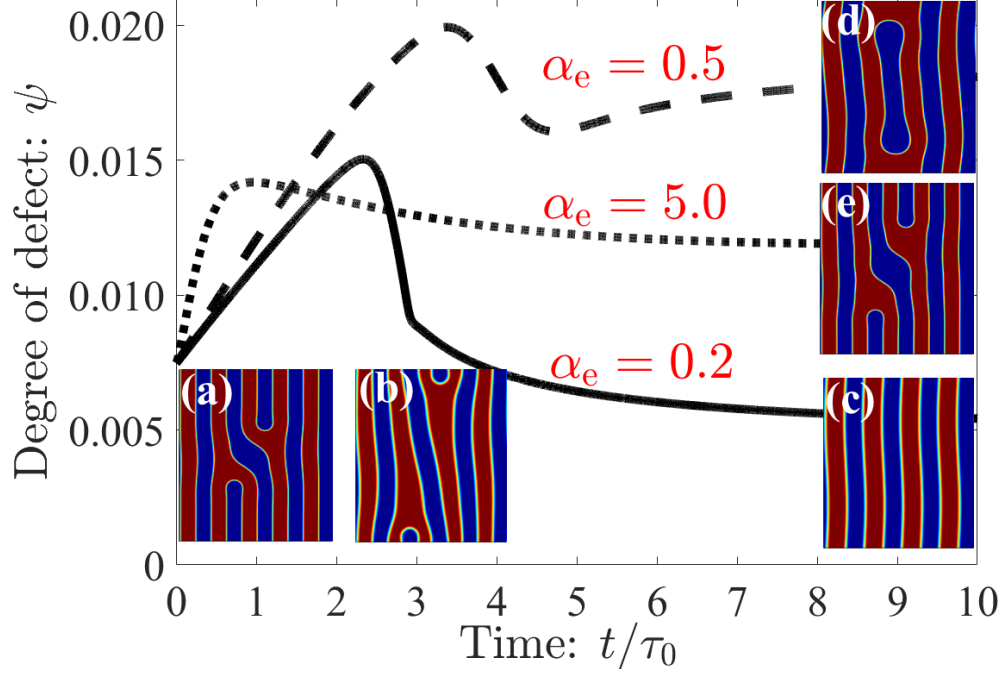


FIG. 4. The temporal evolution of the defect structure (shown in Fig. 1b) of a swollen BCP film at various evaporation rates α_e after annealing time $\tau_a = 0.48\tau_0$ at solvent fraction $\phi_S^{(\text{eq})} = 0.4$ ($< \phi_S^*$). Here, we take $\chi N = 30$, $\phi_S^{(\text{eq})} = 0.4$ ($< \phi_S^*$, corresponding to $\mathcal{R} \approx 1.67$) and $\beta = -1.0$ (in Eq. (6)). The degree of defect is defined by $\psi \equiv \sum_{i,j} (\phi_{i,j} - \phi_{i,1})^2$ (with i, j denoting the sites in the computational box) to quantify the process of defect removal. (Inset) Snapshots of the temporal evolution of the original defect (a) (no solvent) upon different evaporation rates α_e . For slow evaporation, the defect (a) is removed spontaneously to a defect-free state (c) after crossing a transition state (b). In contrast, for faster evaporation, the defect (a) is either kinetically trapped as in (e) or unstable and re-trapped to a new defect state (d).

shear flows [6, 7].

At intermediate swelling ratio $\mathcal{R} \sim 1.7$ (i.e., $\phi_S^{(\text{eq})} \sim 0.4$), the copolymer chains have sufficient mobility and the defect is removed spontaneously if the annealing time τ_a is large enough, as shown in Fig. 3. In SVA experiments, the solvent is usually evaporated after some small annealing time, $\tau_a < \tau_0$. In our simulations, we choose an annealing time $\tau_a = 0.48\tau_0$, after which the solvent is evaporated with controlled rates, τ_e^{-1} . We find that the phase structure of the dried film strongly depends on the evaporation rate $\alpha_e = \tau_e^{-1}/\tau_0^{-1}$ as shown in Fig. 4. The initial defect Fig. 4a can be removed only at *slow* evaporation with $\alpha_e \ll 1$ in

Fig. 4c (a snapshot before the defect is removed is also shown in Fig. 4b). At fast evaporation, $\alpha_e \gg 1$, the defect persists as shown in Fig. 4e, while at intermediate evaporation rates with $\alpha_e \sim 1$, the initial defect becomes unstable but is re-trapped to another defective structure (but with larger spacing) as shown in Fig. 4d.

All these results can be understood in terms of the annealing time τ_a and the evaporation time τ_e . We understand that it is $\tau_a + \tau_e$ that gives the time allowing the copolymers to re-organize during the SVA process (with characteristic time τ_0). For a given small τ_a , when the solvent is removed rapidly, the copolymers lose mobility almost instantly, and are kinetically trapped into the defective swollen morphology. When the solvent is removed gradually, the domain spacing changes and the defects are destabilized; moreover the BCP microdomains have time to relax such that the defects can be removed just as in the case of very long annealing times (without solvent evaporation). In the annealing process of thin BCP films on neutral substrates by non-selective solvents, the most efficient pathway to remove defects is first to swell the film to a sufficiently large solvent fraction where defects become unstable, and only then to evaporate the solvent rapidly when the defect is almost “healed” spontaneously.

In addition, we note that the dependence of the final morphology of dried BCP films on solvent-swelling ratio \mathcal{R} and solvent-evaporation rate α_e can be summarized in a stability diagram of the defect as shown in Fig. 5. Three regions are identified: (I). Stable-defect region at small \mathcal{R} and large α_e , in which the original defect is still stable or metastable and persists in the dried film. (II). Defect-free region at large \mathcal{R} and small α_e , in which the defect becomes unstable and is removed spontaneously. (III). Intermediate-defect region, in which the original defect is unstable but is re-trapped in a new defect state. Such a trapping or transition to a new defect lamellar structure has also been reported in TA of lateral in-plane defect pairs [11, 12] and cross-sectional out-of-plane defect pairs [13] in BCP films.

When the solvent-induced changes in lamellar spacing are negligible (see the inset of Fig. 5), there are only two regions: (I). Stable-defect region, and (II). Defect-free region; the intermediate-defect region (III) does not appear. Moreover, the defect-free region (II) is much smaller when the spacing changes. Note that numerically, the accuracy of the obtained stability diagram depends on the choice of the mesh size; only a small enough mesh size can fully resolve the “shape” of the free-energy landscape and gives accurate stability. Here, we have chosen the mesh size to be $\ell_0 \approx 0.25\lambda_0$ as defined in Eq. (39) which is checked to give

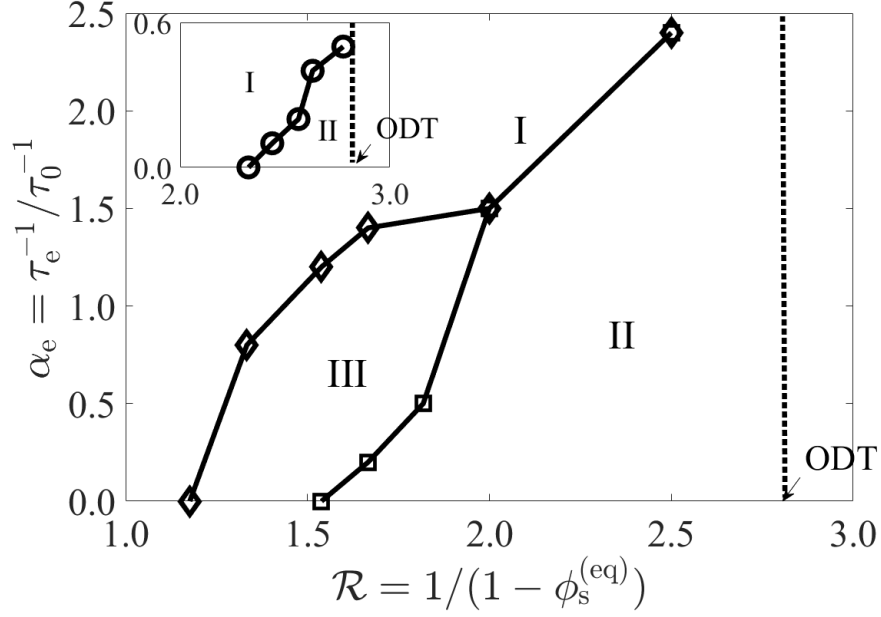


FIG. 5. Stability diagram of the defect shown in Fig. 1b during SVA due to the dilution effects and the changes in lamellar spacing. The diagram is plotted in terms of two parameters: the swelling ratio $\mathcal{R} = 1/(1 - \phi_s^{(eq)})$ and the evaporation rate $\alpha_e = \tau_e^{-1}/\tau_0^{-1}$. Here, we take $\chi N = 30$ and solvent-induced spacing exponent $\beta = -1.0$ (defined in Eq. (6)) as before. The solvent is evaporated after annealing time $\tau_a = 0.48\tau_0$. Three regions are identified: (I). *Stable-defect region* – the original defect is still (meta-) stable. (II). *Defect-free region* – the defect becomes unstable and is removed spontaneously. (III). *Intermediate-defect region* – the original defect is unstable but is re-trapped to a new defect state. The lines are shown to guide the eyes. (Inset) Stability diagram of the defect in the case without spacing changes during SVA.

the same diagram as a smaller mesh size, $0.5\ell_0$. Furthermore physically, the stability of the defect also depends generally on the ratio of the lamellar spacing between swollen state and dry state, which is determined by the swelling ratio \mathcal{R} and the exponent β defined in Eq. (6), which will be discussed in the next section. Our computational prediction agrees, at least qualitatively, with experimental observations [20, 21] that solvent-swelling ratio and the solvent-evaporation rate not only affect the domain spacing of BCPs but also govern the removal of defects or lateral ordering of the BCP microdomains. But the predicted stability diagram should be verified quantitatively in future experiments.

C. Effects of spacing decrease induced by added solvent at large solvent fraction

In this section, we present some more numerical results. As discussed in Sec. II A, the effects of added solvent on the changes of lamellar spacing can be classified into two regimes separated by a crossover solvent volume fraction, ϕ_S^* . In previous sections, we have all taken ϕ_S^* to be very large such that $\phi_S > \phi_S^*$ and lamellar spacing increases with added solvent. Here, we choose small ϕ_S^* and explore the effects of spacing changes in the two regimes, particularly the effects of the spacing decrease with increasing solvent fraction.

We find that, in both regimes, the change in lamellar spacing destabilize the defect, as shown in Figs. 6 and 7. However, the kinetics of defect instability is very different in the two regimes. The solvent-induced spacing increases at small ϕ_S and tends to drive long wavelength structural evolution, as shown in Fig. 3 in the main text. In contrast, the solvent-induced spacing decreases at large ϕ_S and introduces small wavelength undulations, as shown in Fig. 6. Moreover, the kinetically-controlled spacing-increase (when $\phi_S < \phi_S^*$) during solvent annealing is essential for removing BCP defects efficiently, as shown in Fig. 7. Note that the obtained defect-free lamellae adopt a tilted orientation in the xy -plane to adjust to the smaller domain size under the constraints imposed by a fixed $L_x \times L_y$ size of the simulation box.

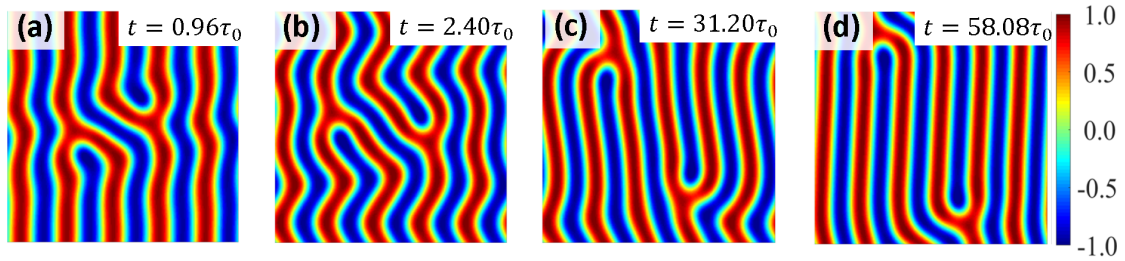


FIG. 6. Destabilization of defects upon instantaneous solvent swelling due to the change of lamellar spacing. Here, we take $\chi N = 30$, $\phi_S^{(\text{eq})} = 0.4$, $\phi_S^* = 0.0$, and $\beta = 1/3$ (defined in Eq. (6)). The lamellar spacing decreases with increasing solvent fraction.

Finally, we would like to point out that at large solvent fraction (over some crossover value ϕ_S^*), the addition of solvent can induce decrease of lamellar spacing in both bulk BCP solutions [34, 35] and BCP films [3, 20, 22]. For example, $\phi_S^* \approx 0.3$ for polystyrene-polyisoprene (PS-PI) copolymer in solutions with non-selective solvent [34]). To explore the effects of solvent induced decrease in lamellar spacing, we have also carried out more

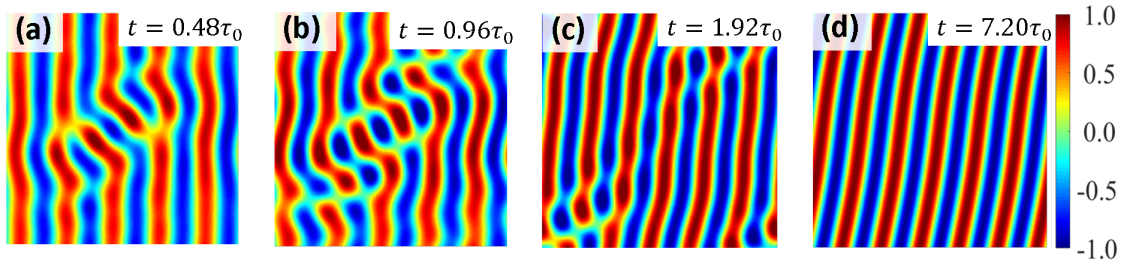


FIG. 7. Destabilization of defects upon instantaneous solvent swelling due to the changes of lamellar spacing. Here, we take $\chi N = 30$, $\phi_S^{(\text{eq})} = 0.6$ and $\phi_S^* = 0.1$. As the solvent fraction increases, the lamellar spacing increases (with an exponent $\beta = -1.0$) when $\phi_S < \phi_S^*$ but decreases (with $\beta = 1/3$) when $\phi_S > \phi_S^*$.

simulations. We find that the solvent-induced spacing decreases at large ϕ_S induces small-wavelength undulations in contrast to the long wavelength structural evolution, as shown in Fig. 3. These small-wavelength undulations are usually not enough to remove defects. Efficient defect removal occurs only for cases with significant spacing-increase during solvent annealing at small solvent fraction (when $\phi_S < \phi_S^*$).

IV. CONCLUSIONS

In summary, we have constructed a two-fluid model to study the microphase separation dynamics of block copolymer (BCP) thin films and applied it to solvent vapor annealing (SVA) processes. We focus on the effects of added (non-selective) solvent on the defect annihilation in ordered BCP thin films on neutral substrates. More specifically, we investigate the solvent-facilitated removal of a typical defect occurring in symmetric lamellar BCP thin films with perpendicular (to the substrate) lamellae.

One of our key findings is that the added solvent not only dilutes the unfavorable interactions between polymer segments, but also changes the characteristic spacing of the BCP lamellae. We find that the solvent-induced increase of the lamellar spacing in dense polymer solution (that is at small solvent volume fraction) facilitates an efficient removal of defects. The kinetic pathways of defect removal during SVA are quite different from that of thermal annealing (TA) and show sensitive dependence on the volume fraction and dynamics of added solvent. The final morphology of the dried BCP film after SVA depend not only on

solvent-swelling ratio \mathcal{R} (or solvent volume fraction) but also solvent-evaporation rate α_e . Such a dependence is summarized in a stability diagram (Fig. 5), which can be verified in future experiments.

Based on these results, we are able to make an important observation about the annealing of thin BCP films on neutral substrates by non-selective solvents. Namely, the most efficient pathway to remove the defects is to first swell the film to a sufficiently large solvent fraction where defects become unstable, and only then to evaporate the solvent rapidly when the defect almost “heals” spontaneously. We believe that the insight provided in this theoretical work on defect removal from perpendicular lamellar BCP thin films by SVA has the potential to greatly expand and diversify the range of applications of solvent-assisted, directed self-assembly of BCP thin films.

We would like to conclude with a few remarks.

(i) *Effects of the dynamics of swelling (solvent uptake).* The swelling dynamics of BCP films strongly depends on the BCP morphology [18, 20]. For example, films with perpendicular lamellae swell faster than parallel lamellae because a higher amount of solvent penetrates through the A/B interfaces that are exposed to the free surface. This effect is associated with the inhomogeneous distribution of solvent within microphase separated film. In this work, we have neglected the coupling of the swelling dynamics with BCP morphology (or phase) dynamics completely. Nonetheless, the inhomogeneous solvent distribution and morphology-dependent swelling rate can have significant effects on the defect removal during solvent annealing process.

(ii) *Structure and dynamics through the film thickness.* In our simulations, we have assumed that the relaxation dynamics through the film thickness is much faster than their lateral dynamics. Based on this assumption, we have neglected any variations of the structure and dynamics through the film thickness completely. However, it has been shown in many experiments that the structure and dynamics through the film thickness can be of importance during SVA processes [1, 3, 18, 20]. For example, as solvent is introduced or removed, there must be a re-distribution of BCP chains in the film and some tilting of the lamellae is expected. Moreover, film thickness is an important parameter, use as a means allowing a direct access to the dynamics of the structural rearrangements [23–25, 30]. By controlling the film thickness in the fully swollen state, Cavicchi et al. [24] found that either parallel or perpendicular cylinder orientation could be obtained. In addition, Kim and Lib-

era [23] suggested that the solvent diffusion to the free surface and the solvent concentration gradients within the film imposed by different solvent evaporation rates are responsible for the different microdomains orientations. More recently, experiments [25] indicated that for a swollen film of parallel cylinder morphology, if the solvent is removed instantaneously, well-ordered parallel cylinders occur; however, if the solvent is removed very slowly, the parallel cylinders reorient and became perpendicular to the substrate. Note that it has been known that surface tension we have neglected also play some important roles in determining the orientation of the lamellae in BCP film [3, 30].

We believe that the insights provided in this theoretical work on defect removal from perpendicular thin BCP films by SVA have the potential to greatly expand and diversify the range of applications of solvent-assisted, directed self-assembly of BCP thin films.

Acknowledgments

We would like to thank S. Komura and T. Qian for discussions and helpful suggestions. This work was supported in part by Grant No. 21822302 and 21434001 of the National Natural Science Foundation of China (NSFC), the joint NSFC-ISF Research Program, jointly funded by the NSFC under Grant No. 51561145002 and the Israel Science Foundation (ISF) under Grant No. 885/15. X. X. was supported by Guangdong Technion – Israel Institute of Technology. D.A. acknowledges the hospitality of the ITP (CAS) and Beihang University, Beijing, China, and a CAS President International Fellowship Initiative (PIFI).

Conflict of Interest

The authors declare no conflict of interest.

Keywords

block copolymer, solvent vapor annealing, defect removal, two-fluid model, Onsager’s variational principle

REFERENCES

- [1] Albert, J.N.; Epps III, T.H. Self-assembly of block copolymer thin films. *Materials Today* **2010**, 13, 24-33.
- [2] Li, W.; Müller, M. Defects in the self-assembly of block copolymers and their relevance for directed self-assembly. *Annu. Rev. Chem. Biomol. Eng.* **2015**, 6, 187-216.
- [3] Sinturel, C.; Vayer, M.; Morris, M.; Hillmyer, M.A. Solvent vapor annealing of block polymer thin films. *Macromolecules* **2013**, 46, 5399-5415.
- [4] Morkved, T.L.; Lu, M.; Urbas, A.M.; Ehrichs, E.E.; Jaeger, H.M.; Mansky, P.; Russell, T.P. Local control of microdomain orientation in diblock copolymer thin films with electric fields. *Science* **1996**, 273, 931-933.
- [5] Thurn-Albrecht, T.; Schotter, J.; Kästle, G.A.; Emley, N.; Shibauchi, T.; Krusin-Elbaum, L.; Guarini, K.; Black, C.T.; Tuominen, M.T.; Russell, T.P. Ultrahigh-density nanowire arrays grown in self-assembled diblock copolymer templates. *Science* **2000**, 290, 2126-2129.
- [6] Marencic, A.P.; Wu, M.W.; Register, R.A.; Chaikin, P.M. Orientational order in sphere-forming block copolymer thin films aligned under shear. *Macromolecules* **2007**, 40, 7299-7305.
- [7] Shelton, C.K.; Jones, R.L.; Epps III, T.H. Kinetics of Domain Alignment in Block Polymer Thin Films during Solvent Vapor Annealing with Soft Shear: An in Situ Small-Angle Neutron Scattering Investigation. *Macromolecules* **2017**, 50, 5367-5376.
- [8] Zhang, X.; Harris, K.D.; Wu, N.L.; Murphy, J.N.; Buriak, J.M. Fast assembly of ordered block copolymer nanostructures through microwave annealing. *ACS Nano* **2010**, 4, 7021-7029.
- [9] Li, W.; Nealey, P.F.; de Pablo, J.J.; Müller, M. Defect removal in the course of directed self-assembly is facilitated in the vicinity of the order-disorder transition. *Phys. Rev. Lett.* **2014**, 113, 168301.
- [10] Hur, S.-M.; Thapar, V.; Ramírez-Hernández, A.; Khaira, G.; Segal-Peretz, T.; Rincon-Delgadillo, P.A.; Li, W.; Müller, M.; Nealey, P.F.; de Pablo, J.J. Molecular pathways for defect annihilation in directed self-assembly. *Proc. Natl. Acad. Sci.* **2015**, 112, 14144-14149.
- [11] Hur, S.M.; Thapar, V.; Ramírez-Hernández, A.; Nealey, P.F.; de Pablo, J.J. Defect annihilation pathways in directed assembly of lamellar block copolymer thin films. *ACS Nano* **2018**, 12, 9974-9981.
- [12] Ren, Y.; Müller, M. Kinetics of pattern formation in symmetric diblock copolymer melts. *J.*

- Chem. Phys.* **2018**, 148, 204908.
- [13] Song, J.-Q.; Liu, Y.X.; Zhang, H.D. Removal pathways of out-of-plane defects in thin films of lamellar forming block copolymers. *Macromolecules* **2018**, 51, 4201-4212.
 - [14] Man, X.; Andelman, D.; Orland, H. Block copolymer films with free interfaces: Ordering by nanopatterned substrates. *Phys. Rev. E* **2012**, 86, 010801.
 - [15] Man, X.; Zhou, P.; Tang, J.; Yan, D.; Andelman, D. Defect-free perpendicular diblock copolymer films: the synergy effect of surface topography and chemistry. *Macromolecules* **2016**, 49, 8241-8248.
 - [16] Baruth, A.; Seo, M.; Lin, C.H.; Walster, K.; Shankar, A.; Hillmyer, M.A.; Leighton, C. Optimization of long-range order in solvent vapor annealed poly (styrene)-block-poly (lactide) thin films for nanolithography. *ACS Appl. Mater. Interfaces* **2014**, 6, 13770-13781.
 - [17] Zhang, J.; Posselt, D.; Sepe, A.; Shen, X.; Perlich, J.; Smilgies, D.M.; Papadakis, C.M. Structural evolution of perpendicular lamellae in diblock copolymer thin films during solvent vapor treatment investigated by grazing-incidence small-angle X-Ray scattering. *Macromol. Rapid Commun.* **2013**, 34, 1289-1295.
 - [18] Zhang, J.; Posselt, D.; Smilgies, D.M.; Perlich, J.; Kyriakos, K.; Jaksch, S.; Papadakis, C.M. Lamellar diblock copolymer thin films during solvent vapor annealing studied by GISAXS: different behavior of parallel and perpendicular lamellae. *Macromolecules* **2014**, 47, 5711-5718.
 - [19] Rudov, A.A.; Patyukova, E.S.; Neratova, I.V.; Khalatur, P.G.; Posselt, D.; Papadakis, C.M.; Potemkin, I.I. Structural changes in lamellar diblock copolymer thin films upon swelling in nonselective solvents. *Macromolecules* **2013**, 46, 5786-5795.
 - [20] X. Gu, *Self-assembly of block copolymers by solvent vapor annealing, mechanism and lithographic applications*, Ph.D. thesis, University of Massachusetts Amherst **2014**.
 - [21] Gu, X.; Gunkel, I.; Hexemer, A.; Gu, W.; Russell, T.P. An in-situ grazing incidence X-Ray scattering study of block copolymer thin films during solvent vapor annealing. *Adv. Mater.* **2014**, 26, 273-281.
 - [22] Gu, X.; Gunkel, I.; Hexemer, A.; Russell, T.P. Controlling domain spacing and grain size in cylindrical block copolymer thin films by means of thermal and solvent vapor annealing. *Macromolecules* **2016**, 49, 3373-3381.
 - [23] Kim, G.; Libera, M. Morphological development in solvent-cast polystyrene-polybutadiene-polystyrene (SBS) triblock copolymer thin films. *Macromolecules* **1998**, 31, 2569-2577.

- [24] Cavicchi, K.A.; Russell, T.P. Solvent annealed thin films of asymmetric polyisoprene-poly lactide diblock copolymers. *Macromolecules* **2007**, 40, 1181-1186.
- [25] Albert, J.N.; Young, W.S.; Lewis III, R.L.; Bogart, T.D.; Smith, J.R.; Epps III, T.H. Systematic study on the effect of solvent removal rate on the morphology of solvent vapor annealed ABA triblock copolymer thin films. *ACS Nano* **2011**, 6, 459-466.
- [26] Paradiso, S.P.; Delaney, K.T.; García-Cervera, C.J.; Cenicerros, H.D.; Fredrickson, G.H. Block copolymer self assembly during rapid solvent evaporation: insights into cylinder growth and stability. *ACS Macro Lett.* **2013**, 3, 16-20.
- [27] Paradiso, S.P.; Delaney, K.T.; García-Cervera, C.J.; Cenicerros, H.D.; Fredrickson, G.H. Cyclic solvent annealing improves feature orientation in block copolymer thin films. *Macromolecules* **2016**, 49, 1743-1751.
- [28] Hur, S.M.; Khaira, G.S.; Ramírez-Hernández, A.; Müller, M.; Nealey, P.F.; de Pablo, J.J. Simulation of defect reduction in block copolymer thin films by solvent annealing. *ACS Macro Lett.* **2015**, 4, 11-15.
- [29] Hannon, A.F.; Bai, W.; Alexander-Katz, A.; Ross, C.A. Simulation methods for solvent vapor annealing of block copolymer thin films. *Soft Matter* **2015**, 11, 3794-3805.
- [30] Hao, J.; Wang, Z.; Wang, Z.; Yin, Y.; Jiang, R.; Li, B.; Wang, Q. Self-assembly in block copolymer thin films upon solvent evaporation: a simulation study. *Macromolecules* **2017**, 50, 4384-4396.
- [31] Helfand, E.; Tagami, Y. Theory of the interface between immiscible polymers. II. *J. Chem. Phys.* **1972**, 56, 3592-3601.
- [32] Lodge, T.P.; Pan, C.; Jin, X.; Liu, Z.; Zhao, J.; Maurer, W.W.; Bates, F.S. Failure of the dilution approximation in block copolymer solutions. *J. Polym. Sci. B* **1995**, 33, 2289-2293.
- [33] Naughton, J.R.; Matsen, M.W. Limitations of the dilution approximation for concentrated block copolymer/solvent mixtures. *Macromolecules* **2002**, 35, 5688-5696.
- [34] Shibayama, M.; Hashimoto, T.; Hasegawa, H.; Kawai, H. Ordered structure in block polymer solutions. 3. Concentration dependence of microdomains in nonselective solvents. *Macromolecules* **1983**, 16, 1427-1433.
- [35] Shibayama, M.; Hashimoto, T.; Kawai, H. Ordered structure in block polymer solutions. 5. Equilibrium and nonequilibrium aspects of microdomain formation. *Macromolecules* **1983**, 16, 1434-1443.

- [36] Huang, C.I.; Lodge, T.P. Self-consistent calculations of block copolymer solution phase behavior. *Macromolecules* **1998**, 31, 3556-3565.
- [37] Netz, R.R.; Andelman, D.; Schick, M. Interfaces of modulated phases. *Phys. Rev. Lett.* **1997**, 79, 1058.
- [38] Tsori, Y.; Andelman, D. Thin film diblock copolymers in electric field: transition from perpendicular to parallel lamellae. *Macromolecules* **2002**, 35, 5161-5170.
- [39] Ciach, A.; Pekalski, J.; Gozdz, W.T. Origin of similarity of phase diagrams in amphiphilic and colloidal systems with competing interactions. *Soft Matter* **2013**, 9, 6301-6308.
- [40] K. Binder, "Phase transitions in polymer blends and block copolymer melts: some recent developments." In *Theories and mechanism of phase transitions, heterophase polymerizations, homopolymerization, addition polymerization*, pp. 181-299, Springer, Berlin, Heidelberg **1994**.
- [41] Majewski, P.W.; Yager, K.G. Rapid ordering of block copolymer thin films. *J. Phys. Condens. Matter* **2016**, 28, 403002.
- [42] Brazovskii, S.A. Phase transition of an isotropic system to a nonuniform state. *J. Exp. Theor. Phys.* **1975**, 41, 85.
- [43] Ohta, T.; Ito, A. Dynamics of phase separation in copolymer-homopolymer mixtures. *Phys. Rev. E* **1995**, 52, 5250.
- [44] Onuki, A. Shear-induced phase separation in polymer solutions. *J. Phys. Soc. Jpn.* **1990**, 59, 3427-3430.
- [45] Doi, M.; Onuki, A. Dynamic coupling between stress and composition in polymer solutions and blends. *Journal de Physique II* **1992**, 2, 1631-1656.
- [46] Milner, S.T. Dynamical theory of concentration fluctuations in polymer solutions under shear. *Phys. Rev. E* **1993**, 48, 3674.
- [47] Buxton, G.A.; Clarke, N. Ordering polymer blend morphologies via solvent evaporation. *EPL* **2007**, 78, 56006.
- [48] Yoo, C.D.; Viñals, J. Anisotropic linear response in block copolymer lamellar phases. *Macromolecules* **2012**, 45, 4848-4856.
- [49] Yabunaka, S.; Ohta, T.; Yoshinaga, N. Self-propelled motion of a fluid droplet under chemical reaction. *J. Chem. Phys.* **2012**, 136, 074904.
- [50] Xu, X.; Thiele, U.; Qian, T. A variational approach to thin film hydrodynamics of binary mixtures. *J. Phys. Condens. Matter* **2015**, 27, 085005.

- [51] Yokoyama, H. Diffusion of block copolymers. *Mater. Sci. Eng. R Rep.* **2006**, 53, 199-248.
- [52] Tu, Y.O.; Drake, R.L. Heat and mass transfer during evaporation in coating formation. *J. Colloid Interface Sci.* **1990**, 135, 562-572.
- [53] J. Crank, *Free and Moving Boundary Problems*, Clarendon Press, Oxford **1987**.
- [54] Liu, F.; Goldenfeld, N. Dynamics of phase separation in block copolymer melts. *Phys. Rev. A* **1989**, 39, 4805.
- [55] Müller, M.; Li, W.; Rey, J.C.O.; Welling, U. Kinetics of directed self-assembly of block copolymers on chemically patterned substrates. *J. Phys. Conf. Ser.* **2015**, 640, 012010.
- [56] Glotzer, S.C., Computer simulations of spinodal decomposition in polymer blends. *Annu. Rev. Comput. Phys.* **1995**, 2, 1-46.

for Table of Contents use only

Defect removal by solvent vapor annealing in lamellar diblock copolymer thin films

Xinpeng Xu, Xingkun Man*, Masao Doi, Zhong-can Ou-Yang, and David Andelman*

